

Semiclassical Origin of Superdeformed Shell Structure in the Spheroidal Cavity Model*

Ken-ichiro Arita

Department of Physics, Nagoya Institute of Technology, Nagoya 466-8555, Japan

Ayumu Sugita and Kenichi Matsuyanagi

Department of Physics, Graduate School of Science, Kyoto University,

Kyoto 606-8502, Japan

(September 2, 1997)

Abstract

Classical periodic orbits responsible for emergence of the superdeformed shell structures for single-particle motions in spheroidal cavities are identified and their relative contributions to the shell structures are evaluated. Both prolate and oblate superdeformations (axis ratio about 2:1) as well as prolate hyperdeformation (axis ratio about 3:1) are investigated. Fourier transforms of quantum spectra clearly show that three-dimensional periodic orbits born out of bifurcations of planar orbits in the equatorial plane become predominant at large prolate deformations, while butterfly-shaped planar orbits bifurcated from linear orbits along the minor axis are important at large oblate deformations.

Typeset using REVTeX

*Submitted to Progress of Theoretical Physics.

I. INTRODUCTION

In the last decade, superdeformed spectroscopy, i.e., study on nuclear structure with large prolate deformations (axis ratio about 2:1), has developed enormously, and further significant progress is expected [1–3].

It is well known that the superdeformation is a result of deformed shell effect and in fact realistic calculations of both Strutinsky-Nilsson type and Hartree-Fock type work well for discussing shell structures observed in experiments at such large deformations [4]. The purpose of this paper, however, is not to make some realistic calculations in relation to recent experimental findings. Rather, we address here to the fundamental question “why nucleus is superdeformed” and investigate semiclassical origin of emergence of the superdeformed shell structure in a simple model, i.e., spheroidal cavity model.

According to the periodic-orbit theory [5–8] based on the semiclassical approximation to the path integral, oscillating parts of single-particle level densities coarse-grained with respect to a certain energy resolution, i.e., shell structure we are interested in, are determined by classical periodic orbits with short periods. As is well known, nucleus favors such shapes at which prominent shell structures are formed and its Fermi surface lies in a valley of the oscillating level density, increasing its binding energy in this way.

With the semiclassical approach, Strutinsky et al. [9] studied the shell structure associated with the spheroidal cavity model and found that planar orbits in the meridian plane are responsible for the shell structure at normal prolate deformations. In addition, they pointed out that some three-dimensional (3D) periodic orbits appearing at large deformations lead to the shell structure responsible for the fission isomers known from seventies, which have superdeformed shapes. As emphasized in Ref. [9], shell structures obtained for the spheroidal cavity model contain basic features, apart from shifts of deformed magic numbers due to the spin-orbit potential, similar to those obtained by the Woods-Saxon potential for heavy nuclei and metallic clusters, and thus it can be used as a simple model in order to understand a semiclassical origin of the emergence of regular oscillating patterns in the coarse-grained quantum spectra at large deformations.

Remarkably, however, two decade after the publication, to the best of our knowledge, little exploration of this idea has taken place and their qualitative argument not fully examined by other researchers, although the spheroidal cavity model has been used for various purposes [10–12]. A paper most relevant to the present paper is that of Frisk [13] who used the periodic-orbit theory and the same cavity model mainly to clarify the origin of the prolate-oblate asymmetry at normal deformations. Although he briefly discussed also the case of large deformations, the importance of 3D orbits was not mentioned.

In this paper, we identify most important periodic orbits that determine major pattern of the oscillating level density at large deformations, including prolate superdeformations, prolate hyperdeformations and oblate superdeformations. For this purpose we make full use of the Fourier transformation method. As briefly reviewed in the text, by virtue of the scaling property of the cavity model, Fourier transforms of quantum spectra exhibit peaks at lengths of classical periodic orbits, enabling us to precisely identify important periodic orbits contributing to the shell structure. This method has been well known [6,8], but not used for the present subject.

Classical periodic orbits in the spheroidal cavity and their bifurcations with variation of

the axis ratio have been thoroughly studied by Nishioka et al. [14,15] This paper may be regarded as a continuation of their work in the sense that we investigate quantum manifestations of these periodic orbits and of their bifurcations. (Actually, this was the intention also of the work by Nishioka et al. [14,15])

We present in section II oscillating parts of smoothed level densities as function of deformation parameter of the cavity. The Fourier transformation method is recapitulated in section III. Periodic orbits and their bifurcations in the spheroidal cavity are briefly reviewed in section IV. Results of semiclassical analysis of shell structures are presented in sections VI, VII and VIII for prolate superdeformations, prolate hyperdeformations and oblate superdeformations, respectively, and conclusions are given in section IX.

A part of this work was previously reported in conference proceedings. [16]

II. OSCILLATING LEVEL DENSITY

We solve the Schrödinger equation for single-particle motions in the spheroidal cavity under the Dirichlet boundary condition. As is well known, the spheroidal cavity is integrable and separable by the spheroidal coordinate system, so that these coordinates are frequently used for solving the Schrödinger equation. We have, however, adopted a spherical-wave decomposition method [17] for this purpose. The reason is merely that we had constructed a computer program based on the latter method for the purpose of efficiently calculating a large number of eigenvalues as function of deformation parameters for cavities of general axially symmetric shapes [18]. In this method, wave functions are expanded in terms of spherical Bessel functions (for radial coordinate) and associated Legendre functions (for polar angle coordinate), and expansion coefficients are determined so as to fulfill the boundary conditions (See Ref. [18,17] for technical details).

The single-particle energy diagram obtained in this way is shown in Fig. 1 as function of deformation parameter δ , which is related to the axis ratio $\eta \equiv a/b$ by $\delta = 3(\eta - 1)/(2\eta + 1)$ in the prolate case and by $\delta = -3(\eta - 1)/(\eta + 2)$ in the oblate case, a and b denoting lengths of the major and the minor axes, respectively, The volume-conservation condition is imposed so that $ab^2 = R_0^3$ in the prolate case and $a^2b = R_0^3$ in the oblate case, R_0 being the radius in the spherical limit.

Figures 2 and 3 display the oscillating part of the smoothed level density in a form of contour map with respect to energy and deformation parameter, which is coarse-grained with the Strutinsky smoothing parameter $\Delta k = 0.5$. We see clearly regular patterns consisting of several valley and ridge structures. Thick solid and broken lines indicate constant-action lines for important periodic orbits responsible for these structures, implication of which will be the major theme in sections VI–VIII.

III. FOURIER TRANSFORM

Single-particle equations of motion for the cavity are invariant with respect to the scaling transformation $(\mathbf{x}, \mathbf{p}, t) \rightarrow (\mathbf{x}, \alpha\mathbf{p}, \alpha^{-1}t)$. The action integral S_r for a periodic orbit r is proportional to the length L_r of it,

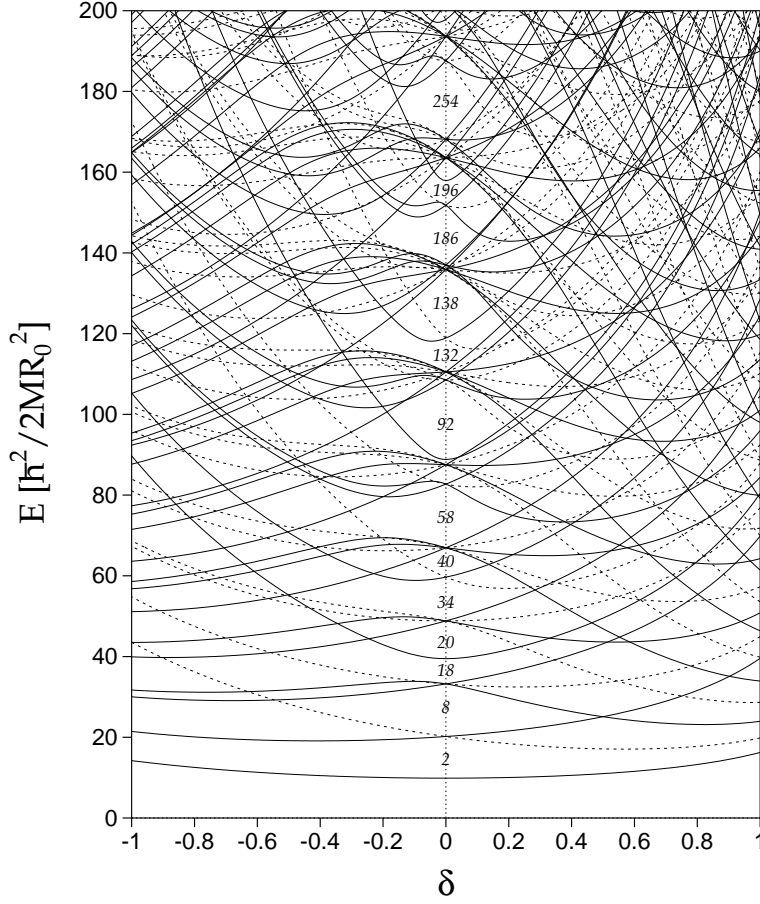


FIG. 1. Single-particle energy diagram for spheroidal cavity, plotted as function of deformation parameter δ . Solid and broken lines represent even- and odd-parity levels. The energy is measured in unit of $\hbar^2/2MR_0^2$, M and R_0 being the mass of a particle and the radius in the spherical limit, respectively. Spin degeneracy factor 2 is taken into account in magic numbers of the spherical limit.

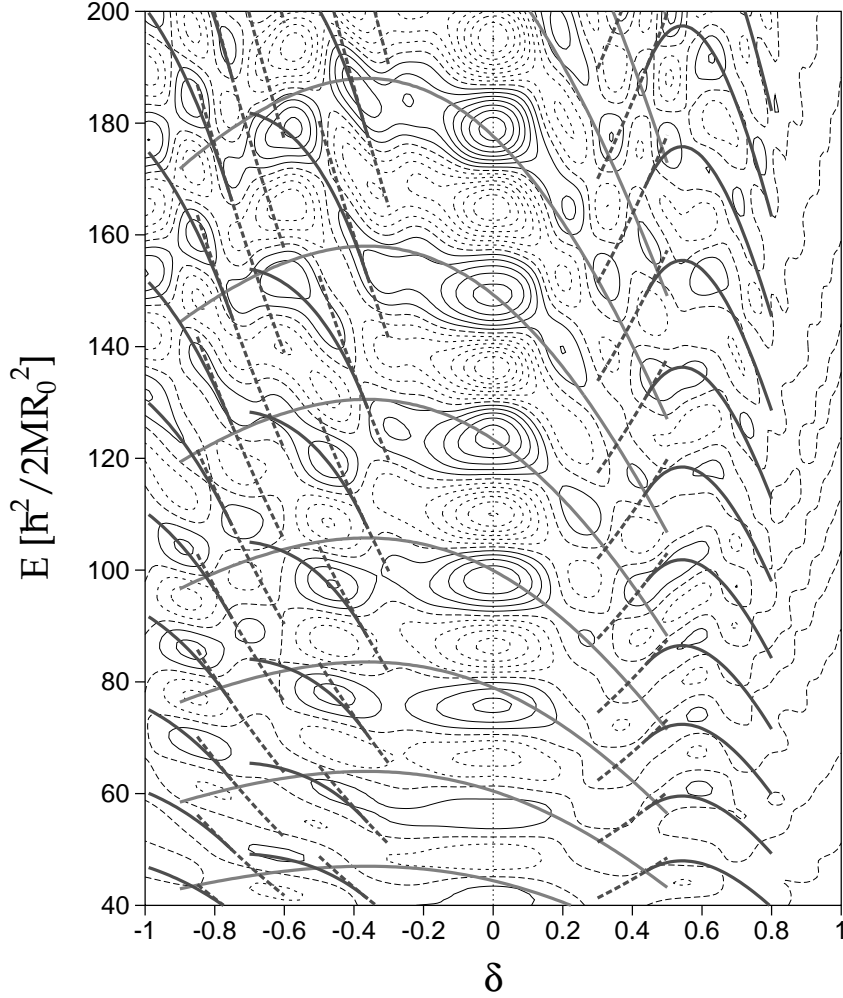


FIG. 2. Oscillating part of the smoothed level density displayed as function of energy and deformation parameter δ . The unit of energy is the same as in Fig. 1. Strutinsky smoothing is taken with smoothing width parameter $\Delta k = 0.5$. Constant-action lines for important periodic orbits are indicated: Thick solid lines running through the spherical closed shells are those for tetragonal orbits in the meridian plane. Thick broken and solid lines in the region $\delta = 0.3 \sim 0.8$ are those for five-point star-shaped orbits in the equatorial plane and for 3D orbits (5:2:1) bifurcated from them, respectively. Broken and solid lines in the region $\delta = -0.3 \sim -0.7$ are those for double repetitions of linear orbits along the minor axis and for butterfly-shaped planar orbits (4:1:1) bifurcated from them, respectively. Likewise, broken and solid lines in the region $\delta = -0.6 \sim -1$ are those for triple repetitions of linear orbits along the minor axis and for planar orbits (6:1:1) bifurcated from them, respectively.

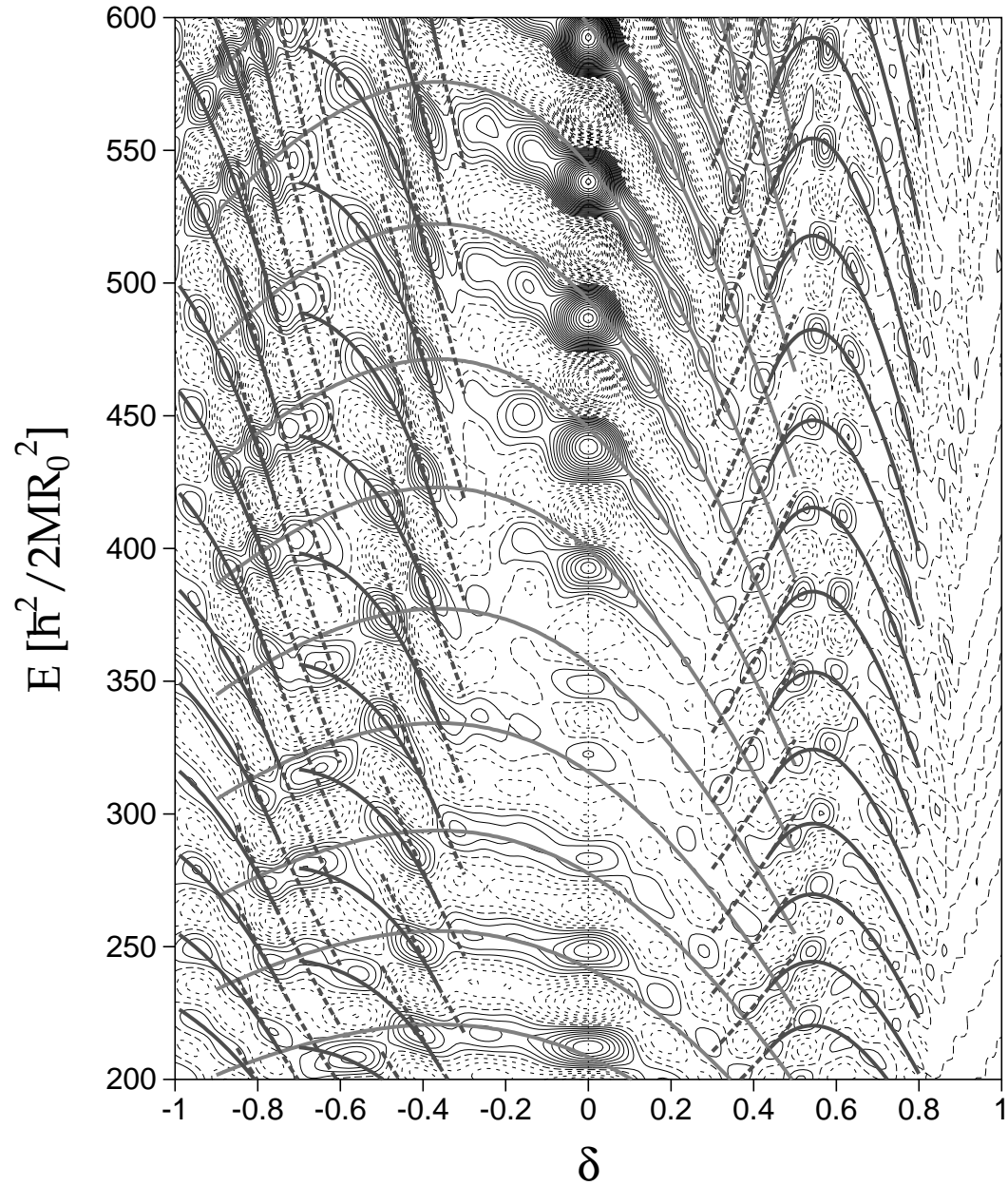


FIG. 3. Same as Fig. 2 but for higher energy region. Much clearer classical-quantum correspondences can be seen.

$$S_r(E = p^2/2M) = \oint_r \mathbf{p} \cdot d\mathbf{q} = pL_r = \hbar kL_r, \quad (1)$$

and the semiclassical trace formula for the level density [5] is written as

$$\begin{aligned} g(E) &= \sum_n \delta(E - E_n) = \frac{M}{\hbar^2 k} \sum_n \delta(k - k_n) \\ &\simeq \bar{g}(E) + \sum_r A_r(k) \cos(kL_r - \pi\mu_r/2), \end{aligned} \quad (2)$$

where $\bar{g}(E)$ denotes the smooth part corresponding to the contribution of *zero-length* orbit, μ_r the Maslov phase of the periodic orbit r . This scaling property enables us to make use of the Fourier transformation of the level density with respect to the wave number k . The Fourier transform $F(L)$ of the level density $g(E)$ is written as

$$\begin{aligned} F(L) &= \int dk e^{-ikL} g(E = \hbar^2 k^2/2M) \\ &\simeq \bar{F}(L) + \pi \sum_r e^{-i\pi\mu_r/2} A_r(i\partial_L) \delta(L - L_r), \end{aligned} \quad (3)$$

which may be regarded as ‘length spectrum’ exhibiting peaks at lengths of individual periodic orbits. [6] In numerical calculation, the spectrum is cut off by Gaussian with cut-off wave number $k_c = 1/\Delta L$ as

$$\begin{aligned} F_{\Delta L}(L) &\equiv \frac{1}{\sqrt{2\pi}\Delta L} \int dL' e^{-\frac{1}{2}(\frac{L-L'}{\Delta L})^2} F(L') \\ &= \frac{M}{\hbar^2} \sum_n \frac{1}{k_n} e^{-\frac{1}{2}(k_n/k_c)^2} e^{-ik_n L} \end{aligned} \quad (4)$$

$$\simeq \bar{F}_{\Delta L}(L) + \pi \sum_r e^{-i\pi\mu_r/2} A_r(i\partial_L) \frac{1}{\sqrt{2\pi}\Delta L} e^{-\frac{1}{2}(\frac{L-L_r}{\Delta L})^2}. \quad (5)$$

IV. PERIODIC-ORBIT BIFURCATIONS

In this section, we recapitulate classical periodic orbits in the spheroidal cavity according to Nishioka et al. [14,15] and Strutinsky et al. [9] We focus our attention on those having short periods.

As is well known, only linear and planar orbits exist in the spherical cavity. When spheroidal deformations set in, the linear(diameter) orbits bifurcate into those along the major axis and along the minor axis. Likewise, the planar orbits bifurcate into orbits in the meridian plane and those in the equatorial plane. Since the spheroidal cavity is integrable, all classical orbits lie on a 3D torus and, in the case of prolate spheroid, periodic orbits are characterized by three positive integers (p, t, q) , which represent numbers of vibrations or rotations with respect to three spheroidal coordinates. They are denoted as $(n_\epsilon, n_\phi, n_\xi)$ and (n_v, n_ϕ, n_u) in Refs. [14,15] and [9], respectively. When the axis ratio η of the prolate spheroid increases, hyperbolic orbits in the meridian plane and three-dimensional orbits are successively born through bifurcations of linear and planar orbits in the equatorial plane. Bifurcations occur when the following condition is satisfied:

$$\eta \equiv \frac{a}{b} = \frac{\sin(\pi t/p)}{\sin(\pi q/p)}. \quad (6)$$

As we shall see in succeeding sections, most important orbits for superdeformed shapes (axis ratio about 2:1) are 3D ones having ratio $(p:t:q) = (p:2:1)$ with $p = 5, 6, 7, \dots$ etc. They bifurcate from planar orbits that turns twice ($t = 2$) about the symmetry axis. Likewise, planar orbits with (4:2:1) bifurcate from linear orbits that repeat twice along the minor axis. These new-born orbits resemble the Lissajous figures of the superdeformed harmonic oscillator with frequency ratio $\omega_{\perp}:\omega_z = 2:1$. Every bifurcated orbits form continuous families of degeneracy two, which means that we need two parameters to specify a single orbit among continuous set of orbits belonging to a family having a common value of action integral (or equivalently, length).

For prolate hyperdeformed shapes (axis ratio about 3:1), bifurcations from linear and planar orbits that turns three times ($t = 3$) about the symmetry axis are important. The new-born orbits are hyperbolic orbits in the meridian plane (6:3:1) and 3D orbits $(p:3:1)$ with $p = 7, 8, 9, \dots$ etc.

In the case of oblate spheroidal cavities, periodic orbits are classified in Ref. [15] into two modes; whispering-gallery (W) mode and bouncing-ball (B) mode. Systematics of periodic-orbit bifurcations in the W-mode is similar to the prolate case and can be treated just by exchanging the role of t and q . On the other hand, B-mode orbits are successively created through bifurcations of multiple repetitions of linear orbits along the minor axis, when the following condition is satisfied:

$$\eta \equiv \frac{a}{b} = \frac{1}{\sin(\pi t/p)}. \quad (7)$$

Bifurcations of this kind do not depend on q , so that, for instance, planar orbits (4:1:1) are created simultaneously with two families of 3D orbits (4:1:3/2) and (4:1:2). (For B-mode orbits, half integer values of q are allowed as well as integers, due to different definition of integration range for the action integral related to q ; see Ref. [15])

Bifurcation points and variations of lengths with deformation are displayed for some short periodic orbits in Table I and Fig. 4.

V. SHELL STRUCTURE AND CONSTANT-ACTION LINE

Using the trace formula, we can extract informations about classical periodic orbits from the Fourier transforms of the level density. In this section we discuss another way of using the trace formula, i.e., the constant-action line analysis. [9] As stated in the above section (see Eq. (2)), the quantum level density can be represented as the summation over periodic orbits. If a few orbits having nearly the same action integral dominate in the sum, it is expected that valleys in the contour map of the oscillating part of the smoothed level density versus energy E and deformation δ are characterized by constant-action lines $S(E, \delta) = \text{const.}$ for those dominant orbits. The equation for such lines is $kL_r - \pi\mu_r/2 = (2n + 1)\pi$, namely,

$$E(\delta) = \frac{1}{2M} \left(\frac{2\pi\hbar(n + 1/2 + \mu_r/4)}{L(\delta)} \right)^2, \quad (n = 0, 1, 2, \dots). \quad (8)$$

TABLE I. Bifurcation points of periodic orbits specified by $(p:t:q)$ in the spheroidal cavity. Only those for short orbits to be discussed in sections VI–VIII are displayed.

orbit $(p:t:q)$	axis ratio (a/b)	deformation δ	orbit length in R_0
(4:2:1)	1.414	0.325	7.127
(5:2:1)	1.618	0.438	8.101
(6:2:1)	1.732	0.492	8.654
(7:2:1)	1.802	0.523	8.995
(8:2:1)	1.848	0.542	9.220
(6:3:1)	2.0	0.6	9.524
(7:3:1)	2.247	0.681	10.421
(8:3:1)	2.414	0.728	11.011
(9:3:1)	2.532	0.758	11.437
(4:1:1)	1.414	-0.364	6.350
(6:1:1)	2.0	-0.75	7.560

As an example, let us examine the shell structure at normal deformations $|\delta| \lesssim 0.3$. In this region, triangular and tetragonal orbits in the meridian plane give dominant contributions to the level density. This fact was first pointed out by Strutinsky et al. [9] (Although the triangular orbits were overlooked there, actions of the two families of orbits scale in the same way as function of deformation so that their argument was correct in essence.) The Fourier amplitudes at lengths of some meridian-plane orbits are plotted in Fig. 5 as function of deformation parameter δ . We see that the meridian-plane orbits are important for small δ and their contributions decline with increasing $|\delta|$. In Figs. 2 and 3, constant-action lines (8) for the tetragonal orbits in the meridian plane are indicated. The period of the shell oscillation is mainly determined by the tetragonal orbits, and the valley structure of the level density at normal deformation is nicely explained by the constant-action lines of them. We also notice that the intensity of spherical shell structure is weakened at $E \sim 300$ and the phase of valley is shifted from that of the constant-action lines for $E \simeq 250$ –350. This is due to the supershell effect associated with the interference of the triangular and tetragonal orbits. [6,19]

In this way, we can analyze the properties of the shell structure through classical periodic orbits. In the following sections, we shall utilize these techniques in order to identify dominant classical periodic orbits that characterize the shell structures in superdeformed shapes.

VI. PROLATE SUPERDEFORMATIONS

Figure 6 displays Fourier transforms of quantum spectra for prolate spheroidal cavities with deformation parameter $\delta = 0.1 \sim 0.6$. At normal deformations with $\delta = 0.1$, as mentioned in the previous section, we notice peaks associated with the triangular and tetragonal orbits in the meridian plane. With increasing deformation, bifurcations of linear and planar

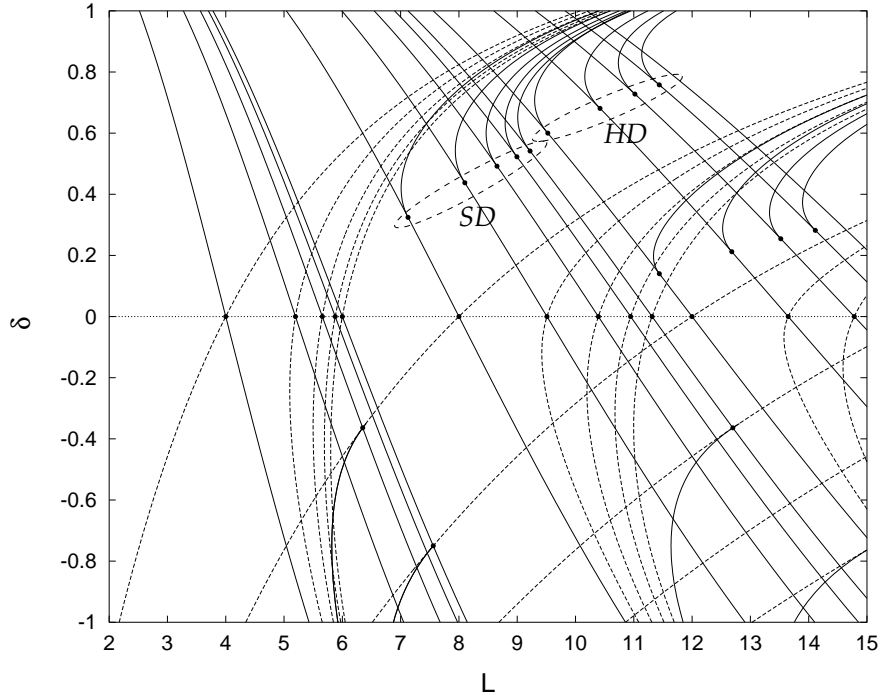


FIG. 4. Variations of lengths of periodic orbits specified by $(p:t:q)$ in the spheroidal cavity with respect to deformation parameter δ . Only those for short orbits to be discussed in sections VI–VIII are displayed. For a more complete diagram, see Nishioka et al. [14,15]

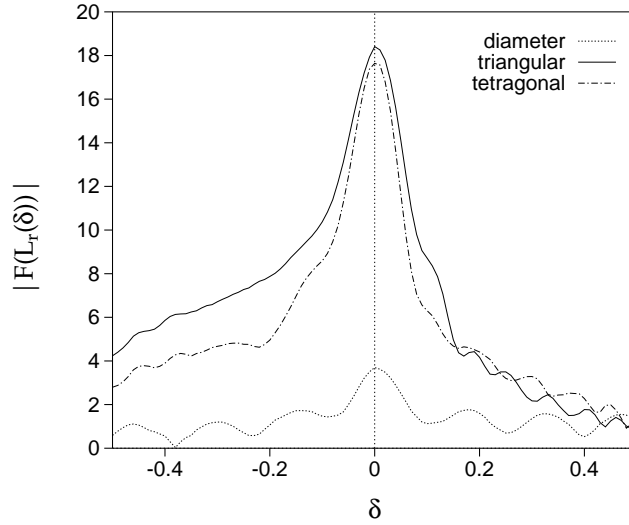


FIG. 5. Absolute values of the Fourier amplitudes defined in Eq. (4), at lengths $L = L_r$ of some short meridian-plane orbits, plotted as functions of deformation parameter δ .

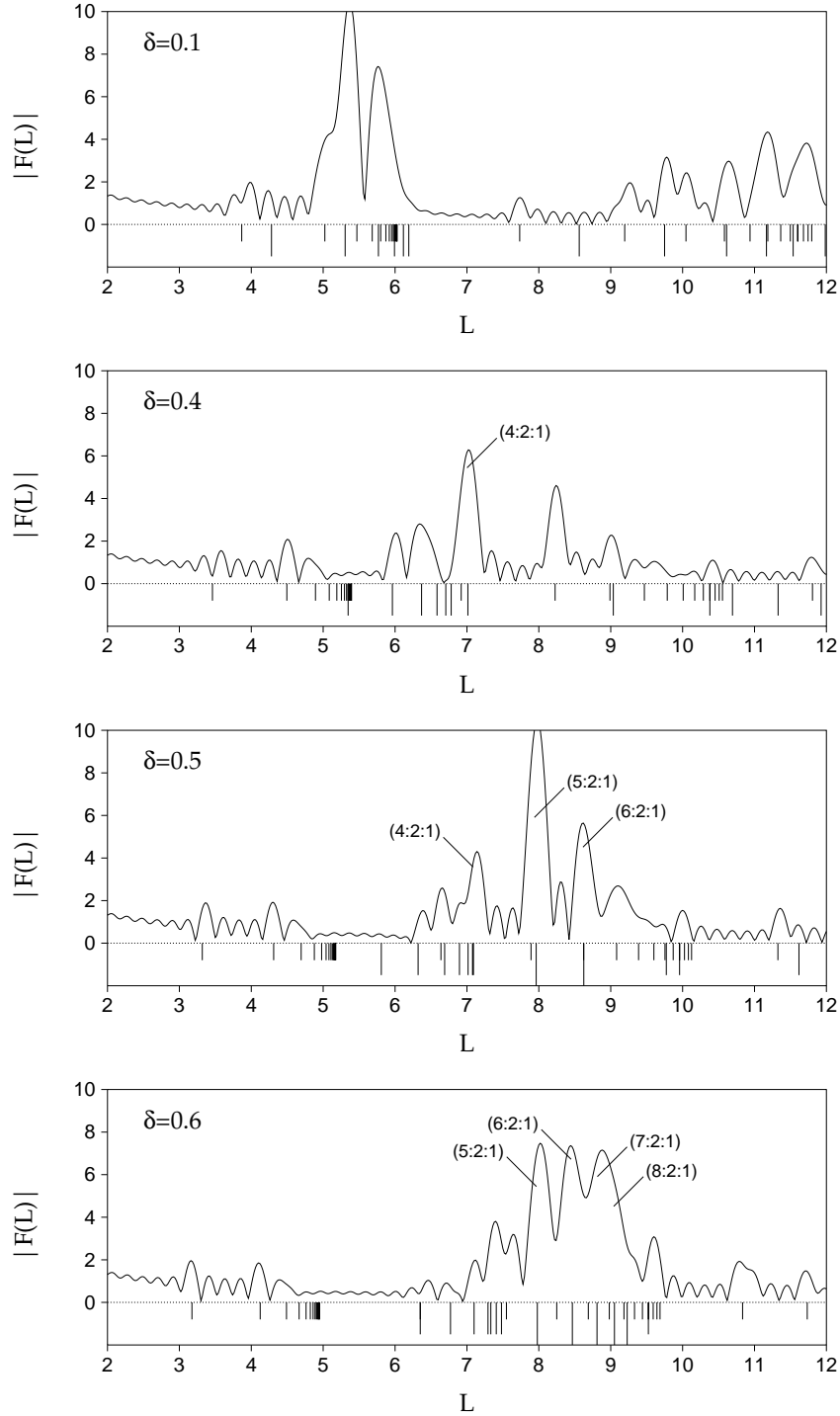


FIG. 6. Length spectra, i.e., Fourier transforms of quantum level densities, for spheroidal cavities with deformation parameter $\delta = 0.1, 0.4, 0.5$ and 0.6 . Cut-off wave number $k_c = \sqrt{600}$ is used in Eq. (4). In the bottoms of every figures, lengths of classical periodic orbits are indicated by vertical lines. Long, middle and short vertical lines are used for 3D orbits, planar orbits in the meridian and the equatorial planes, respectively.

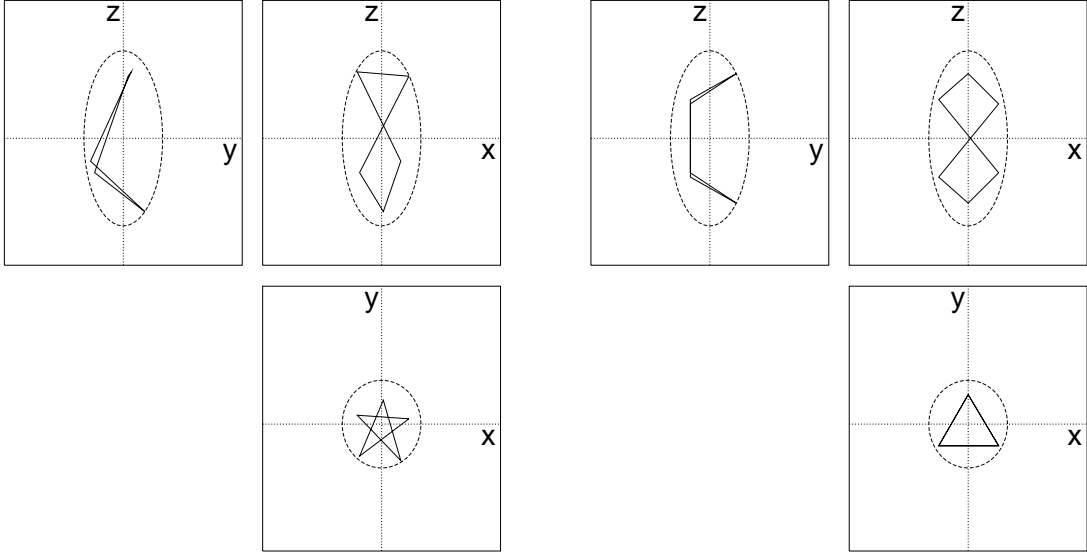


FIG. 7. Three-dimensional orbits (5:2:1) and (6:2:1) in the superdeformed prolate cavity with deformation $\delta = 0.6$ (axis ratio $\eta = 2$). Their projections on the (x, y) , (y, z) and (z, x) planes are displayed.

orbits in the equatorial plane successively take places. Thus, the highest peak at $L \simeq 7$ of the Fourier transform for $\delta = 0.4$ is associated with butterfly-shaped planar orbits with $(p:t:q) = (4:2:1)$, that bifurcate at $\delta \simeq 0.32$ from double repetitions of linear orbits along the minor axis. For $\delta = 0.5$, the prominent peak at $L \simeq 8$ and 8.6 correspond to 3D orbits (5:2:1) and (6:2:1) bifurcated respectively from five-point star-shaped orbits and double traversals of triangular orbits in the equatorial plane. With further increase of δ , same kinds of 3D orbits successively bifurcate from equatorial-plane orbits. For $\delta = 0.6$ (axis ratio $\eta = 2$), peaks around $L \simeq 9$ are associated with 3D orbits (7:2:1) and (8:2:1) that are bifurcated from 7-point star-shaped orbits and double traversals of rectangular orbits in the equatorial plane.

In Figs. 2 and 3, constant-action lines for the 3D orbits (5:2:1) are indicated. Good correspondence is found between these lines and the valley structure seen in the superdeformed region with δ around 0.6. Thus we can conclude that the bifurcations of equatorial orbits play essential roles in the formation of the superdeformed shell structure, and it is characterized by the 3D orbits $(p:2:1)$.

Some of these 3D orbits are displayed in Fig. 7. They possess similarities with the figure-eight shaped orbits in the superdeformed harmonic oscillator with frequency ratio $\omega_{\perp}:\omega_z = 2:1$. An important difference between the cavity model under consideration and the harmonic oscillator model should be noted, however: In the former those periodic orbits exist for all deformation parameters δ larger than the bifurcation points, whereas in the latter such orbits appear only for special deformations corresponding to rational ratios of the major and the minor axes.

On the other hand, magnitudes of contributions of individual orbits are found to exhibit remarkable deformation dependence. Namely, Fourier peak heights associated with new orbits created by bifurcations quickly increase with increasing deformation and reach the

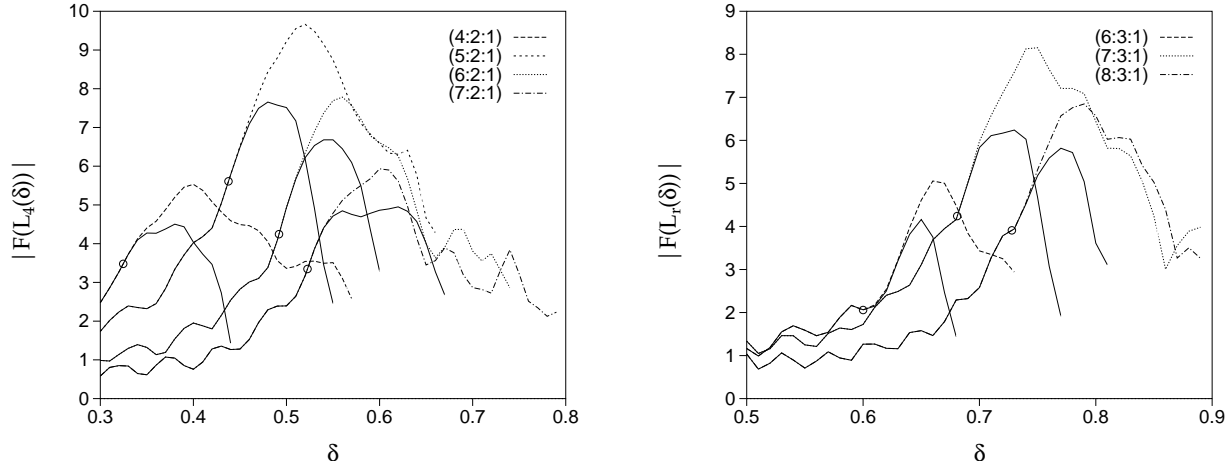


FIG. 8. Same as Fig. 5 but for meridian-plane hyperbolic orbits and 3D orbits ($p:2:1$) (left-hand side) and ($p:3:1$) (right-hand side). Solid lines are those for equatorial-plane orbits from which these orbits are bifurcated.

maxima. Then, they start to decline. This behavior is apparently seen in Fig. 6. Figure 8 displays deformation dependence of the Fourier amplitudes $|F(L)|$ defined in Eq. (4) at lengths $L = L_r$ for some classical periodic orbits, which confirms the behavior noted above. This behavior has not been pointed out in the previous papers. It should be emphasized that relative magnitudes and deformation dependence of contributions of individual periodic orbits found here are significantly different from those roughly estimated in Ref. [9].

To get deeper understanding on the mechanism of the enhancements associated with bifurcations noted above, semiclassical approximation that goes beyond the stationary phase approximation used in deriving the trace formula (2) may be required. Such a semiclassical theory applicable for three dimensional deformed cavities is not available at present and remains as a challenging subject for future.

VII. PROLATE HYPERDEFORMATIONS

Figure 9 displays Fourier transforms for $\delta = 0.7$ and 0.8 . For $\delta \simeq 0.7$, the peak at $L \simeq 10.3$ is associated with 3D orbits (7:3:1) bifurcated from 7-point star-shaped orbits in the equatorial plane. For $\delta = 0.80$, we see a rise of peak at $L \simeq 10.8$, which is associated with 3D orbits (8:3:1) bifurcated from 8-point star-shaped orbits in the equatorial plane. They are displayed in Fig. 10. These 3D orbits resemble with the Lissajous figures of the hyperdeformed harmonic oscillator with frequency ratio $\omega_{\perp}:\omega_z = 3:1$. In the same manner as for the 3D orbits responsible for superdeformations, Fourier peak heights associated with these new-born orbits rapidly increase after the bifurcations, reach the maxima and then decline with increasing deformation (see Fig. 8). Thus, also in this case, bifurcations of equatorial orbits, but of different types ($p:3:1$), play the major role in the formation of this shell structure.

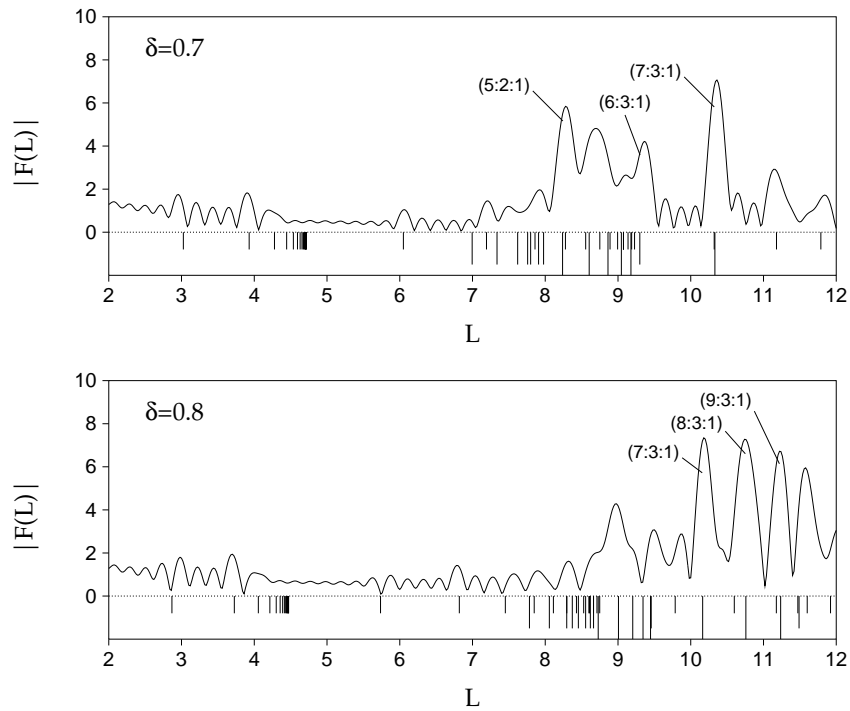


FIG. 9. Same as Fig. 6 but for $\delta = 0.7$ and 0.8 (axis ratio $\eta \simeq 2.3$ and 2.7).

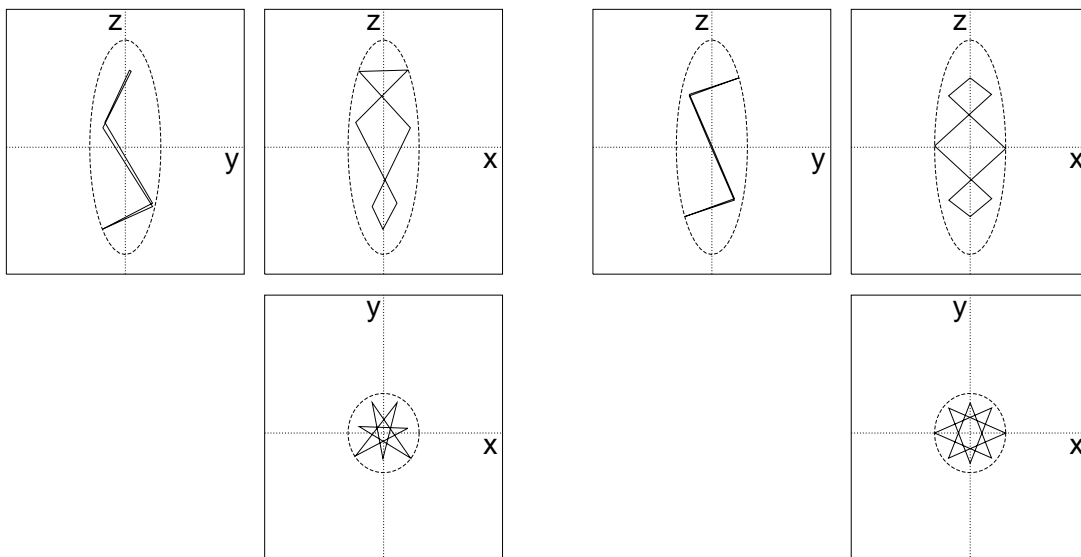


FIG. 10. Same as Fig. 7 but for 3D orbits $(7:3:1)$ and $(8:3:1)$ in the hyperdeformed prolate cavity with deformation $\delta = 0.8$.

VIII. OBLATE SUPERDEFORMATIONS

Finally let us consider oblate deformations. Figure 11 displays Fourier transforms of quantum spectra for oblate spheroidal cavities with $\delta = -0.3 \sim -0.85$. For $\delta = -0.3$, dominant two peaks are associated with triangular and tetragonal orbits in the meridian plane. For $\delta = -0.4$, we see a dominant peak at $L \simeq 6.3$ in addition to the peaks associated with the meridian-plane orbits. This new peak is associated with the butterfly-shaped planar orbits (4:1:1) bifurcated from double repetitions of linear orbits along the minor axis.

At $\delta = -0.75$ (axis ratio $\eta = 2$), the other peak at $L \simeq 7.5$ becomes important. This peak is associated with the triple traversals of linear orbits along the minor axis, which bifurcate just at this shape to the planer hyperbolic orbits (6:1:1). They make predominant contribution for $\delta = -0.85$ (the peak at $L \simeq 7.1$).

Constant-action lines for these bifurcated orbits (4:1:1) and (6:1:1) are indicated in Figs. 2 and 3. We see clear correspondence between shapes of these lines and of valleys in the oscillating level density. Combining this good correspondence with the behavior of the Fourier peaks mentioned above, it is evident that these periodic orbits are responsible for the shell structure at oblate superdeformations with axis ratio about 2:1. According to the classification in section IV, these are W-mode orbits.

In contrast to W-mode orbits, B-mode 3D orbits do not seem very important, although those with $(p:t:q) = (5:1:2), (6:1:2), \dots$ etc. are already bifurcated from equatorial-plane orbits at the superdeformed region. This is an important difference between the prolate and the oblate superdeformations in the spheroidal cavity model.

IX. CONCLUSIONS

Classical periodic orbits responsible for emergence of the superdeformed shell structure for single-particle motions in spheroidal cavities are identified and their relative contributions to the shell structures are evaluated. Both prolate and oblate superdeformations as well as prolate hyperdeformations are investigated.

Fourier transforms of quantum spectra clearly show that 3D periodic orbits born out of bifurcations of planar orbits in the equatorial plane become predominant at large prolate deformations, while butterfly-shaped planar orbits bifurcated from linear orbits along the minor axis are important at large oblate deformations.

Good correspondence between constant-action lines for these periodic orbits and valley structures in the oscillating part of the smoothed level density confirms the above conclusions.

After writing this paper, we learned that Magner et al. [20] had carried out an extensive semiclassical analysis of shell structure in large prolate cavities. In their work, a rather large coarse-graining parameter γ for the level density was used, so that the equatorial-orbit bifurcations discussed in this paper were not clearly seen. It remains as a challenge for future to develop a semiclassical theory capable of treating the equatorial-orbit bifurcations, and the phase-space trace formula proposed in Ref. [20] seems to provide a general framework for this aim.

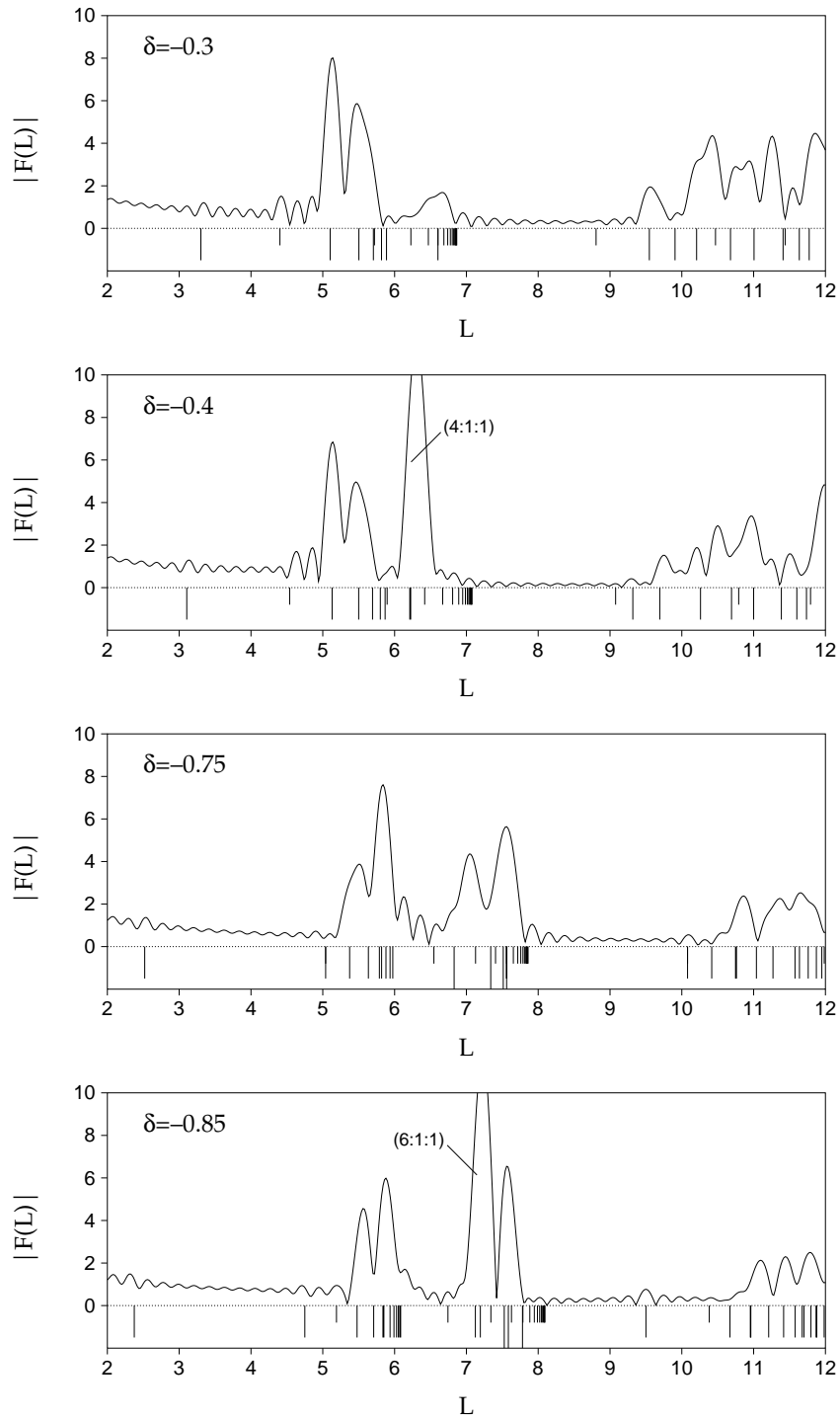


FIG. 11. Same as Fig. 6 but for oblate cavities with $\delta = -0.3 \sim -0.85$.

ACKNOWLEDGMENTS

We thank Matthias Brack, Alexander Magner, Zhang Xizhen, Rashid Nazmitdinov and Masayuki Matsuo for stimulating conversations.

REFERENCES

- [1] P. J. Nolan and P. J. Twin, *Ann. Rev. Nucl. Part. Sci.* **38** (1988), 533.
- [2] R. V. F. Janssens and T. L. Khoo, *Ann. Rev. Nucl. Part. Sci.* **41** (1991), 321.
- [3] *Proceedings of the Workshop on Gammasphere Physics*, ed. M. A. Deleplanque, I. Y. Lee and A. O. Macchiavelli (World Scientific, 1996).
- [4] S. Åberg, H. Flocard and W. Nazarewicz, *Ann. Rev. Nucl. Part. Sci.* **40** (1990), 439.
- [5] M. C. Gutzwiller, *J. Math. Phys.* **12** (1971), 343.
- [6] R. Balian and C. Bloch, *Ann. Phys.* **69** (1972), 76.
- [7] M. V. Berry and M. Tabor, *Proc. R. Soc. London* **A349** (1976), 101.
- [8] M. Brack and R. K. Bhaduri, *Semiclassical Physics* (Addison-Wesley, Reading, 1997).
- [9] V. M. Strutinsky, A. G. Magner, S. R. Ofengenden and T. Døssing, *Z. Phys.* **A283** (1977), 269.
- [10] R. Arvieu, F. Brut, J. Carbonell and J. Touchard, *Phys. Rev.* **A35** (1987), 2389.
- [11] Y. Ayant and R. Arvieu, *J. of Phys.* **A20** (1987), 397.
- [12] R. Arvieu and Y. Ayant, *J. of Phys.* **A20** (1987), 1115.
- [13] H. Frisk, *Nucl. Phys.* **A511** (1990), 309.
- [14] H. Nishioka, M. Ohta and S. Okai, *Mem. Konan Univ. Sci. Ser.*, **38(2)** (1991), 1.
- [15] H. Nishioka, N. Nitanda, M. Ohta and S. Okai, *Mem. Konan Univ. Sci. Ser.*, **39(2)** (1992), 67.
- [16] K. Arita, A. Sugita and K. Matsuyanagi, *Proc. Int. Symp. on Similarities and Differences between Nuclei and Clusters*, Tsukuba, July 1–4, 1997, AIP Conference Proceedings 416, ed. Y. Abe, I. Arai, S. M. Lee and K. Yabana, p. 393.
Proc. Int. Symp. on Atomic Nuclei and Metallic Clusters: Finite Many-Fermion Systems, Prague, Sep. 1–5, 1997, *Czech. J. of Phys.* **48** (1998), 821.
Proc. Int. Conf. on Nuclear Structure and Related Topics, Dubna, Sep. 9–13, 1997, ed. S. N. Ershov, R. V. Jolos and V. V. Voronov, p. 198.
- [17] T. Mukhopadhyay and S. Pal, *Nucl. Phys.* **A592** (1995), 291.
- [18] A. Sugita, K. Arita and K. Matsuyanagi, preprint KUNS1431 (1997), *Prog. Theor. Phys.* **100** (1998), in press.
- [19] H. Nishioka, Klavs Hansen and B. R. Mottelson, *Phys. Rev.* **B42** (1990), 9377.
- [20] A. G. Magner, S. N. Fedotkin, F. A. Ivanyuk, P. Meier, M. Brack, S. M. Reimann, and H. Koizumi, *Ann. Physik* **6**, (1997), 555.
 see also A. G. Magner, S. N. Fedotkin, F. A. Ivanyuk, P. Meier and M. Brack, *Proc. Int. Conf. on Atomic Nuclei and Metallic Clusters: Finite Many-Fermion Systems*, Prague, Sep. 1–5, 1997, *Czech. J. of Phys.* **48** (1998), 845.